PROCEEDINGS, 42nd Workshop on Geothermal Reservoir Engineering
Stanford University, Stanford, California, February 13-15, 2017
SGP-TR-212

Modeling of Hydraulic Fracture Propagation at the kISMET Site Using a Fully Coupled 3D Network-Flow and Quasi-Static Discrete Element Model

Jing Zhou[1], Hai Huang[1*], Earl Mattson[1], Herb F. Wang[2], Bezalel C. Haimson[3], Thomas W. Doe[4], Curtis M. Oldenburg[5], Patrick F. Dobson[5]

1. Energy and Environmental Science & Technology Directorate, Idaho National Laboratory, PO Box 1625, Idaho Falls, ID 83415

2. Department of Geoscience, University of Wisconsin-Madison, 1215 West Dayton Street, Madison, WI 53706

3. Geological Engineering, University of Wisconsin-Madison, 1509 University Avenue, Madison, WI 53706

4. FracMan Technology Group, Golder Associates Inc., 18300 Union Hill Road, Suite 200, Redmond, WA 98052

5. Energy Geosciences Division, Lawrence Berkeley National Laboratory, 1 Cyclotron Road, Berkeley, CA 94720

*corresponding author, E-mail address: Hai.Huang@inl.gov

Keywords: Modeling, Hydraulic Fracturing, Quasi-static DEM

ABSTRACT

Aimed at supporting the design of hydraulic fracturing experiments at the kISMET site, ~1500 m below ground in a deep mine, we performed pre-experimental hydraulic fracturing simulations in order to estimate the breakdown pressure, propagation pressure, fracture geometry, and the magnitude of induced seismicity using a newly developed fully coupled three-dimensional (3D) network flow and quasi-static discrete element model (DEM). The quasi-static DEM model, which is constructed by Delaunay tessellation of the rock volume, considers rock fabric heterogeneities by using the "disordered" DEM mesh and adding random perturbations to the stiffness and tensile/shear strengths of individual DEM elements and the elastic beams between them. A conjugate 3D flow network based on the DEM lattice is constructed to calculate the fluid flow in both the fracture and porous matrix. One distinctive advantage of the model is that fracturing is naturally described by the breakage of elastic beams between DEM elements. It is also extremely convenient to introduce mechanical anisotropy into the model by simply assigning orientation-dependent tensile/shear strengths to the elastic beams.

In this paper, the 3D hydraulic fracturing model was verified against the analytic solution for a penny-shaped crack model. We applied the model to simulate fracture propagation from a vertical open borehole based on initial estimates of rock mechanical properties and in-situ stress conditions. The breakdown pressure and propagation pressure are directly obtained from the simulation. In addition, the released elastic strain energies of individual fracturing events were calculated and used as a conservative estimate for the magnitudes of the potential induced seismic activities associated with fracturing. The comparisons between model predictions and experimental results are still ongoing.

1. INTRODUCTION

Enhanced geothermal system (EGS) energy production relies on the ability to create fractures with desired size, aperture, orientation and connectivity, which in turn depend on understanding of fracture propagation mechanisms, knowledge of subsurface stress conditions, rock properties, formation permeability and design of operational strategies such as wellbore placement and injection rate, fracture fluid properties, etc. The difficultly of characterizing these properties and monitoring fracture geometry evolution currently limits the development of advanced adaptive control of fractures for permeability management. In order to address those challenges and uncertainties of subsurface energy-related processes involving fracturing and permeability enhancement, earth scientists from several national laboratories and three universities have carried out a $1.35 M project to develop a new underground facility called kISMET (permeability (k) and Induced Seismicity Management for Energy Technologies) at the Sanford Underground Research Facility (SURF) in Lead, South Dakota (see a recent report by Oldenburg et al., 2016).

An important part of the kISMET experimental design is the determination of the injection parameters (duration of injection at given flow rate) to produce hydraulic fractures with desired size ranges for their intended purposes. For the stress-measurement fracturing tests (which were done at depths of 54-97 m below the drift invert), it was important to assure that the fractures are large enough to be representative of the stress field and produce reasonable stress values, but not so large that they penetrate into the main kISMET experiment volume, which is approximately 40 m (131 *ft*) below the drift invert (floor) around the five-spot wellbore pattern. For the stimulation experiment, it was important to create fractures large enough to have a reasonable geophysical signature, but not so large that they would extend significantly beyond the monitoring array.

The second objective of design calculations is to provide an initial conservative estimate of the magnitudes of potential seismic activities induced by the hydraulic fracturing experiments under various injection scenarios. Vibration and seismicity were pointed out as a concern by SURF because of potential negative effects on other experiments being carried out at SURF.

2. METHODOLOGY OF COUPLED NETWORK FLOW – DEM MODEL

Hydraulic fracture propagation in crystalline low-permeability rocks is a very complex process, controlled by many factors, e.g., *in-situ* stress state, injection rate, fluid viscosity, and rock heterogeneity across many scales, ranging from mineral fabrics to natural fractures of varying sizes, and mineral fillings, and to the scales of larger stratigraphic layers. Very often the generated fracture morphology is difficult to monitor and characterize over time during the fracturing experiments in the field through existing diagnostic methods. Thus the development of physics-based hydraulic fracturing models not only provides valuable information to guide fracturing experiment design and monitoring planning, but also helps interpret experimental results and monitoring data. A robust hydraulic fracturing model should at least include the following physics:

(1) stress concentration and redistribution before, during, and after fracture propagation;
(2) pressure dissipation due to viscous flow along discrete fractures and within the formation, and due to leak-off from fractures into the formation;
(3) appropriate coupling between fracture opening and fluid flow.

There have been a number of hydraulic fracturing models with varying levels of physics rigor developed using different analytical and numerical approaches (Economides and Nolte, 2000; Xu et al., 2010; Dahi-Taleghani and Olson, 2011; Huang et al., 2016; Fu et al., 2013; Wu and Olson, 2013). Each method has its own advantages and disadvantages (Jing, 2003). In this project, a coupled network flow and quasi-static discrete element model (DEM) developed and implemented into INL's FALCON code for coupled subsurface thermo-hydro-mechanical-chemical (THMC) processes was applied for pre-test fracturing design purposes because it provides a nice balance between simulation run time and rigor of modeled physics.

The coupled network flow and quasi-static DEM model is briefly described in this section. The discrete element method originally introduced by Cundall and Strack (1979) provides the most broadly applicable and versatile approach to modeling the initiation, coalescence, and propagation of micro-cracks and macroscopic fracturing process. In order to simplify the explanations, we will use the 2D model to illustrate the method and algorithm. As shown in by Figure 1, the rock volume is represented by an assemblage of randomly generated, non-uniform-sized circular (in 2D) and spherical elements (often referred as DEM particles). The DEM lattice (Figure 1a) is formed by connecting adjacent DEM particles with elastic beams. In 3D, a Delaunay tessellation scheme is used to decompose the domain into non-overlapping, disordered tetrahedra with each vertex representing a DEM particle and each edge representing an elastic beam connecting two adjacent DEM particles. A conjugate flow lattice (as shown in Figure 1b) is then constructed accordingly. The coupling between fluid flow and fracture propagation is represented naturally, since the flow nodes are more-or-less aligned with the potential fracture propagation direction.

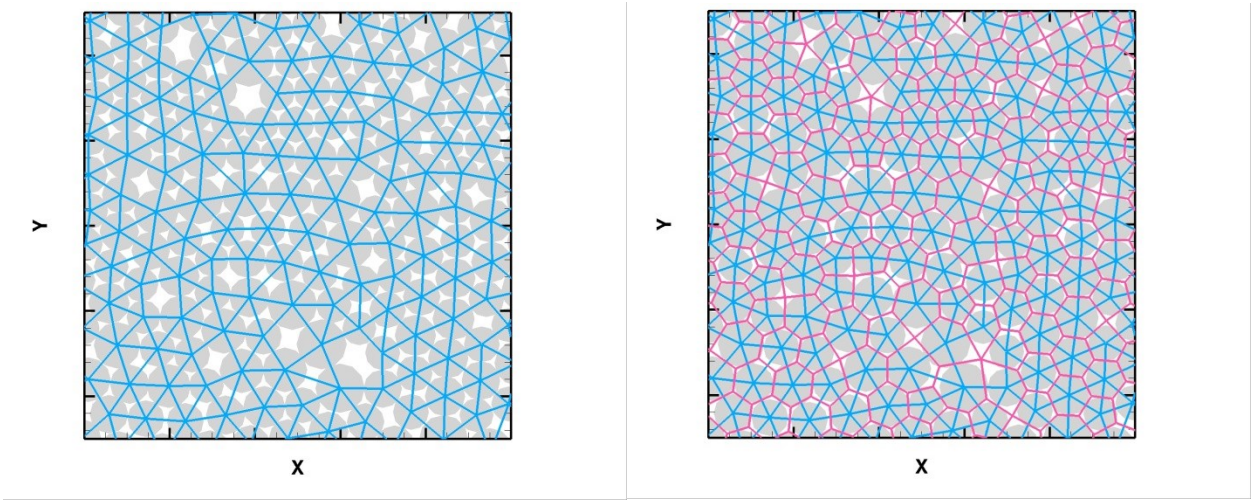

(a) DEM lattice **(b) DEM lattice coupled with flow lattice**

Figure 1: The concept and construction of the dual lattice system in 2D. In both figures, the gray circles represent randomly distributed DEM particles. The blue lines (elastic beams) connecting DEM particles represent the DEM lattice. The red lines in (b) are the conjugate flow lattice.

In a quasi-static DEM model with a mechanical load applied, particles will move and rotate into a new mechanical equilibrium stage via a numerical relaxation procedure (similar to successive over-relaxation procedures). The elastic beams between two adjacent particles will be deformed (stretching, bending, and twisting) and sustain increasing stretching and shearing forces. Once the shearing and stretching forces of a beam exceed some pre-defined threshold values, that beam will break, mimicking a crack initiation, and the stress will be transmitted into neighboring beams, which are likely to break sequentially, mimicking crack propagation.

During each time step, this beam breaking—relaxation process is repeated a number of times until no more beams break at the given loading level, at which point the simulation progresses to the next time step. Unlike the other DEM-based fracture simulators like PFC2D or PFC3D from Itasca, Inc. (Potyondy and Cundall, 2004) that are fully dynamic, the hydraulic fracture propagation is treated

here as a quasi-static process. Given the fact that the rates of mechanical deformation and relaxation are usually much faster than the rates of fluid pressure diffusion, it is reasonable to expect that such quasi-static models can be used to simulate the hydraulic fracturing process in EGS. The biggest advantage of such quasi-static treatment of the hydraulic fracturing process is that it allows the use of large time steps in the simulation, compared to the fully dynamic approaches in which time-step sizes are limited for stability reasons, i.e., the time-step size has to be smaller than the time required for an elastic wave to travel through one element, which significantly increases simulation run times. Another significant advantage of the quasi-static DEM model is that the beam breaking—relaxation procedure ensures the system will rapidly converge to a global minimum of the free energy of the system for a given load during each time step. In order to account for the local mechanical heterogeneities due to variations of mineral fabrics, random perturbations can be added to the tensile strength, shear strength, and stiffness constant of individual beams. It turns out that the randomness of the beam mechanical strengths, together with the "disordered" DEM lattice, are critical for generating realistic fracture geometries and fracture patterns.

The displacement and rotation of each DEM particle may result from the combined effects of the following forces leading to the formation of hydraulic fractures:

(1) beam force and moment from the connected particles;
(2) viscous damping force;
(3) repulsion through contact of neighboring particles not connected by beams
(4) external force caused by the fluid pressure gradient due to injection.

Figure 2 depicts the force calculation steps used in the DEM model (Zhou et al., 2015). Because this method is quasi-static, the dynamic step with calculation of velocity and acceleration is not required. The Force-Displacement law is used to determine both the translational and rotational motion of each particle and the contact forces after particle displacement.

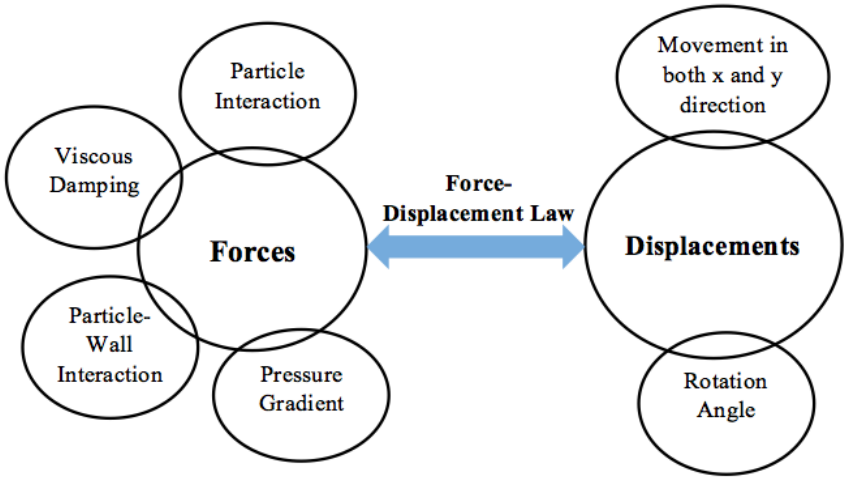

Figure 2: The algorithm of quasi-static DEM model.

In the absence of a pressure gradient, the force and moment exerted on a node *i* by a neighboring node *j* are given by

$$\vec{F}_{i,j} = k_n(d_{i,j} - d^0_{i,j})\vec{n}_{i,j} + k_s\frac{1}{2}(\phi_{i,j} + \phi_{j,i})\vec{s}_{i,j}, \quad (1)$$

$$M_{i,j} = k_s d_{i,j}[\frac{\Phi}{12}(\phi_{i,j} - \phi_{j,i}) + \frac{1}{2}(\frac{2}{3}\phi_{i,j} + \frac{1}{3}\phi_{j,i})]. \quad (2)$$

Here k_n and k_s are the normal and shear force constants, $d_{i,j} = |\vec{x}_i - \vec{x}_j|$ is the distance between the centers of two DEM nodes (the centers of the corresponding particles), *i* and *j*, and $d^0_{i,j} = r_i + r_j$ is the initial equilibrium (stress free) distance, where r_i is the radius of the i^{th} particle. $\vec{n}_{i,j}$ and $\vec{s}_{i,j}$ are the unit vectors parallel and perpendicular to the center line connecting nodes *i* and *j*, $\phi_{i,j}$ is the rotation angle in the local frame of the beam, $\vec{t}_{i,j}$ is the unit vector parallel to the tangent of the bent beam at node *i*. For an isotropic elastic medium, there are two independent elastic constants, the two Lame coefficients (usually represented by λ and μ) or the Young's

modulus E_0 and shear modulus G_0 are commonly used. If a regular square or triangular lattice is used in the simulation, an isotropic two dimensional elastic medium with known Young's modulus and shear modulus can be simulated by using model parameters k_n, k_s and Φ given by $k_n = E_0 A / d$, $k_s = 12E_0 I[d^2(1+\Phi)]$ and $\Phi = 12E_0 I / G_0 A d^2$, where A is the cross-sectional area of the elastic beam and I is the geometric part of its moment of inertia. The normal and shear force constants, k_n and k_s, must be calibrated against the desired Young's modulus E and Poisson's ratio ν. The detailed calibration process can be found in Section 3.2. In addition, $\Phi = (12EI)/(GAd^2)$, in which I is moment of inertia, G is shear modulus, and A is the cross-section area of the elastic beam.

Once a mechanical load is applied (the load is imposed by the injection of fluids in this case), an over-relaxation algorithm is used to relax the DEM network to a new state of mechanical equilibrium in which the net forces and moments are zero for all of the DEM particles. If a beam satisfies the von Mises failure criterion given by

$$\tau = \left(\frac{\varepsilon}{\varepsilon_c}\right)^2 + \frac{\max\left(|\phi_{i,j}|,|\phi_{j,i}|\right)}{\phi_c} > 1 \tag{3}$$

it will be irreversibly removed from the DEM network, giving rise to crack initiation and growth. Here ε is the longitudinal tensile strain of the beam, and ε_c is the critical longitudinal tensile strain (the maximum tensile strain that the bond can sustain), and ϕ_c is the critical rotational angle above which the beam will break, even in the absence of tensile strain. Typical values for ε_c and ϕ_c (dimensionless) range from ~10^{-4} to ~10^{-2} for rocks and many other polycrystalline brittle solids. This criterion can simulate both tensile- and shear-induced rock failure.

In order to couple fluid flow with the DEM model while appropriately accounting for viscous pressure dissipation along fractures (approximated by Couette flow between parallel plates) and through the formation (Darcy flow) due to leak-off of hydraulic fracturing fluids, a conjugate flow lattice is constructed based on the DEM lattice, as illustrated in the 2D example of Figure 1(b). Conjugate nodes are assigned to the centers of polygons (2D DEM lattice) and tetrahedrons (3D DEM lattice). The flow lattice is formed by connecting the neighboring conjugate nodes. Assuming Darcy flow is valid, the governing equation for fluid flow is

$$\frac{\partial(\varphi\rho_f)}{\partial t} = \nabla\left(\frac{\rho_f k}{\mu}\nabla p\right) + Q \tag{4}$$

where φ is the porosity of the porous medium, ρ_f is the density of the injected fluid, k is the formation permeability, μ is the fluid's dynamic viscosity, p is the pressure, and Q is the injection rate. Fluid pressure at each conjugate flow node is updated during each time step. Any pressure alteration will exert additional force on the neighboring DEM particles as equivalent body forces through the following equations

$$\vec{F}_{i,j} = k_n(d_{i,j} - d_{i,j}^0)\vec{n}_{i,j} + k_s\frac{1}{2}\left(\phi_{i,j} - \phi_{j,i}\right)\vec{s}_{i,j} - \nabla p \cdot \pi r^2 \tag{5}$$

$$\vec{M}_{i,j} = k_s d_{i,j}\left[\frac{\Phi}{12}\left(\phi_{i,j} - \phi_{j,i}\right) + \frac{1}{2}\left(\frac{2}{3}\phi_{i,j} + \frac{1}{3}\phi_{j,i}\right)\right] \tag{6}$$

It is important to note that before a crack is initiated, the coupled network flow-DEM model reproduces the conventional poroelasticity effect. When an elastic beam breaks, a more conductive flow channel will be generated that connects the two associated fluid nodes of the flow network with a new permeability in the form of

$$k \cong \frac{b^2}{12} \tag{7}$$

where b is the aperture of the fracture (same as the separation distance of the two neighboring DEM particles that have been "cleaved", a direct output of DEM model). The new permeability will replace the original value and is used in the pressure simulations. The leakage from fractures into adjacent porous matrix is accounted for by connecting the flow nodes along the fractures with the flow nodes within the porous matrix, unlike most other boundary element models that typically only account for fluid flow along fractures. This unique feature allows FALCON to evaluate the leakage of fracturing fluid into the porous matrix.

The simulation of the coupled network flow-DEM processes consists of interleaved fluid flow, mechanical relaxation of the DEM network, and beam-breaking steps. During each time step, the new fluid pressure field (in both fractures and matrix) is obtained first by solving Eq. 3. Then the new fluid pressure field is applied to the DEM network according to Eqs. 5-6, and the DEM network is relaxed to a new mechanical equilibrium. The beam that most exceeds the failure criteria, which is usually near a crack tip, is then removed from the DEM network and the network is again relaxed into a new state of mechanical equilibrium. The mechanical relaxation and beam-breaking are repeated a number of times during each time step, mimicking crack initiation and propagation, until no additional beam-breaking occurs, at which point the simulation proceeds to a new time step. This quasi-static approach to modeling hydraulic

fracturing is reasonable because stress build-up and relaxation associated with hydraulic fracture propagation often exhibits quasi-static behavior.

3. MODEL CALIBRATION

3.1 Calibration Parameters

The DEM model parameters, normal force constant (k_n), shear force constant (k_s), critical tensile strain (ε_c), and critical rotational angle (ϕ_c) must be calibrated to accurately represent the mechanical properties of brittle rocks such as Young's modulus (E), Poisson's ratio (ν), tensile strength (σ_T) and compressive strength (σ_c) (Huang and Mattson, 2014). Tables 1 & 2 list the geological and operational parameters chosen for pre-fracturing test simulations, based on the results of Vigilante (2016), who summarized current knowledge of stresses and rock mechanical properties at the SURF site.

Table 1. Rock properties and operational parameters used in the simulations.

Parameters	Value
Young's modulus (GPa)	41
Poisson's ratio	0.23
Shear Modulus (GPa)	17.9
Density (g/cm^3)	2.95
Uniaxial Compressive Strength (MPa)	115
Uniaxial Tensile Strength (MPa)	14
Formation Permeability (nanoDarcy)	10
Formation Porosity	0.06
Injection Rate (liter/min = lpm)	2.0
Injection Fluid Viscosity (Pa.s)	$1.0\text{x}10^{-3}$ ($0.89\text{x}10^{-3}$ for water at 25°C)

Table 2. Estimated *in-situ* principal stresses from compilations of Vigilante (2016).

Principal Stress	σ_v	σ_{Hmax}	σ_{Hmin}
Value (MPa)	44	30.35	25.07

3.2 Calibration – Uniaxial Tension Test

The calibration of DEM model parameters is performed by simulating a uniaxial tensile test, as shown in Figure 3. Because the hydraulic fracture opening and propagation are mainly driven by the tensile failure at the fracture tip caused by increased pore pressure, we calibrate the DEM to Young's modulus, Poisson's ratio, and tensile strength.

The dimensionless force constant k_n was selected from a random Gaussian distribution with a mean of $\mu = 1.0$ and a standard deviation of $\sigma = 0.1$. A constant k_s/k_n ratio of 0.3 was used in the parameter calibration. The force constant k_n and k_s/k_n jointly determine the macroscopic Young's modulus and Poisson's ratio. The critical tensile strains ε_c of the beams were selected randomly from a Gaussian distribution with a mean of $\mu = 1 \times 10^{-3}$ and a standard deviation of $\sigma = 1 \times 10^{-4}$. The critical tensile strain determines the macroscopic tensile strength of the rock. During the numerical uniaxial tension test, DEM particles near both ends move uniformly in opposite directions at a specified strain rate in order to mimic uniaxial tensile loading conditions. At each loading stage, the average axial stress and lateral strain within the sample were calculated by volume averaging in order to generate the stress-strain curve.

Figure 3 shows the simulated stress-strain curves for the uniaxial tensile test. The simulated rock sample behaves like a linear elastic solid before the load reaches its peak failure value corresponding to the linear parts of the stress-strain curves. When the load reaches its peak (failure) value, the sample fails suddenly and stress is released rapidly. This brittle behavior is typical for crystalline rocks. The stress-strain curve gives the dimensionless Young's modulus (average slope of the linear parts of the curve) of $E_0 = 2.0$. The simulated sample has a macroscopic dimensionless critical tensile stress of 1.43×10^{-3}. The dimensionless critical tensile stress can then be rescaled to the dimensional macroscopic, measureable tensile strength of the rock through Eq. 8. The tensile strength used in the model for pre-test simulations is higher than the reported value from the literature (~15 *MPa*) in order to provide initial conservative estimates of the breaking pressure. We plan to calibrate the model using laboratory core test data in the future.

$$\sigma_T = \frac{E}{E_0}\sigma_{T0} = \frac{41.3\,GPa}{2.0} \square 1.43 \square 10^{-3} = 29.3\,MPa \tag{8}$$

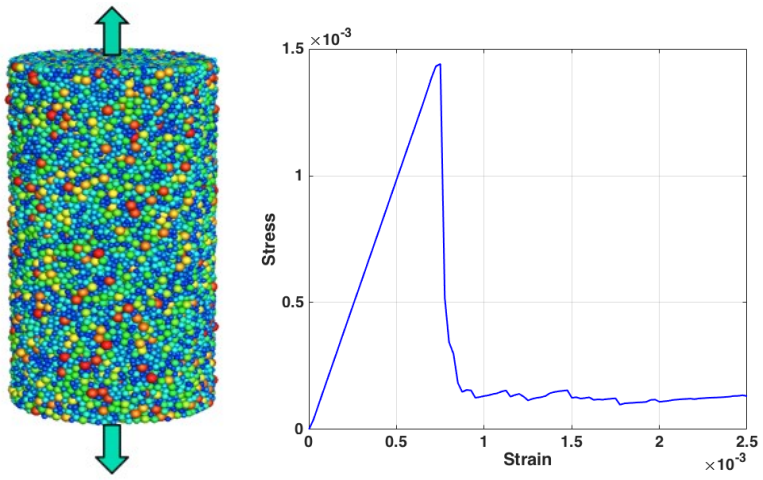

Figure 3: Numerical uniaxial tension test: (left) the DEM model used in the test (color scales with particle size) and (right) simulated dimensionless stress-strain curve for the uniaxial tension test.

An important part of the kISMET experimental design is the determination of the injection parameters (duration of injection at given flow rate and pressure) to produce hydraulic fractures with desired size ranges for their intended purposes. For the stress-measurement fracturing, it was important to assure that the fractures are large enough to be representative of the stress field and produce reasonable stress values, but not so large that they penetrate into the main kISMET experiment volume, which is approximately 40 m (131 *ft*) below the drift invert (floor) around the five-spot pattern. For the stimulation experiment, it was important to create fractures large enough to have a reasonable geophysical signature, but not so large that they would extend significantly beyond the monitoring array, which was deployed in boreholes that are about 3 m away from the central test borehole.

4. PRE-TEST SIMULATION RESULTS

In the pre-test simulations, we assumed that the rocks are homogeneous in a statistical sense (local variations of beam stiffness, and tensile and shear strengths are included via random perturbations), isotropic, and the model domain size is chosen to be 50 *ft* × 50 *ft* × 30 *ft*, (15.24 *m* on a side) as shown in Figure 4. An open vertical wellbore is located at the center of the model domain and penetrates the whole depth (red cylinder) with an arbitrarily chosen diameter of 1 *ft* (0.3048 m) for pre-test simulations. Only the middle part of the vertical well (green zone) of height 3 *ft* (0.91 *m*) takes the fluid injection with the rate of 2 *L/min*. The actual wellbore diameter and length of the injection interval are smaller (see a recent report by Oldenburg et al., 2016), and will be used in future post-test simulations. The overburden stress (σ_v) is oriented in the *Z*-direction, and the maximum compressive horizontal stress (σ_{Hmax}) is oriented in the *Y*-direction. The values of *in situ* stresses used in the simulations are given in Table 2. A total of 118,634 DEM particles of variable sizes, ranging from 0.4 *ft* to 0.6 *ft* (0.12 *m* to 0.18 *m*) were randomly generated and packed into the model domain to form the DEM lattice and associated conjugate flow network. The permeability of the rock is 10 nanoDarcy (1.0×10^{-20} m^2), representing an ultralow-permeability formation.

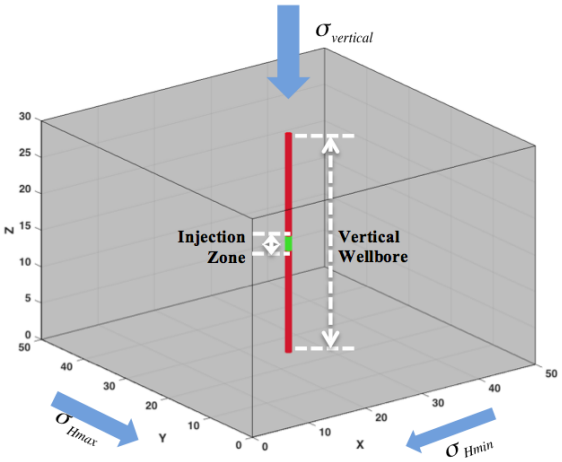

Figure 4: Simulated domain with a vertical open wellbore.

Figure 5 shows the simulated fracture propagation process with time. As the fluid injection starts, the pressure in the wellbore begins to rapidly build up due to the low compressibility of water. Once the wellbore pressure is large enough (~35 seconds after injection starts, or equivalently, after ~1.17 L of injection have occurred) to break the beams between DEM particles adjacent to the wellbore, a nearly vertical fracture is initiated and starts to propagate (Figure 5b). One important observation worth mentioning is that once the fracture starts to initiate, it will "pop-open" a crack with a relatively large radius initially, ~1.2 m, with an average aperture of ~2.0×10^{-4} m. These predicted values are similar to analytical calculations presented in chapter 7 of Oldenburg et al. (2016). Due to the local mechanical heterogeneity incorporated into the model, the initial crack does not assume an ideal bi-wing penny shape, but rather it exhibits some asymmetry. As more fluid is injected, the crack continues to propagate more or less along the horizontal maximum compressive stress direction (Y-axis in the simulation) and eventually grows into a penny shape (see Figure 5c – Figure 5d). Unlike the uniform crack-front growth, the simulated growth of the crack front at any given moment is actually non-uniform, with some parts of the crack front growing and the rest periodically static. The uniform growth concept is valid only in a statistical sense during the late stages of crack propagation. Also, because there is randomness introduced into the mechanical properties of beams, the fracture propagation is not perfectly symmetric at both sides, which is realistic for natural rock considering the heterogeneity in the subsurface environment. The generated crack surface versus injected fluid volume is summarized in Table 3. The crack radius also matches with the analytical solution (see Oldenburg et al., 2016). The numerical model result shows a similar trend to the analytical solution for fracture radius vs. injection volume.

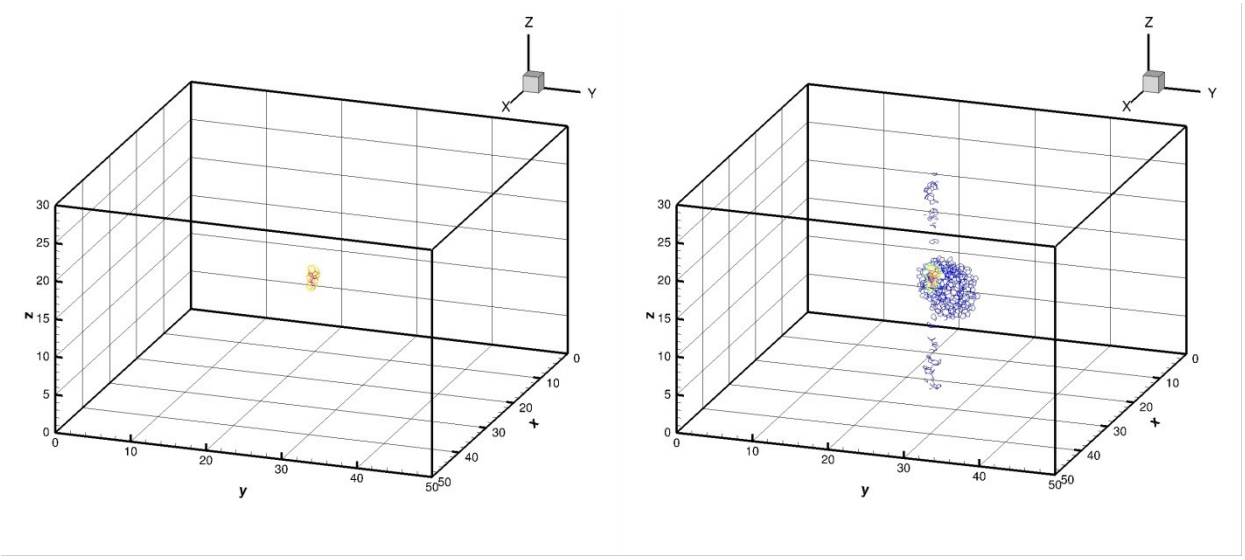

(a) t = 0 s (b) t = 35s

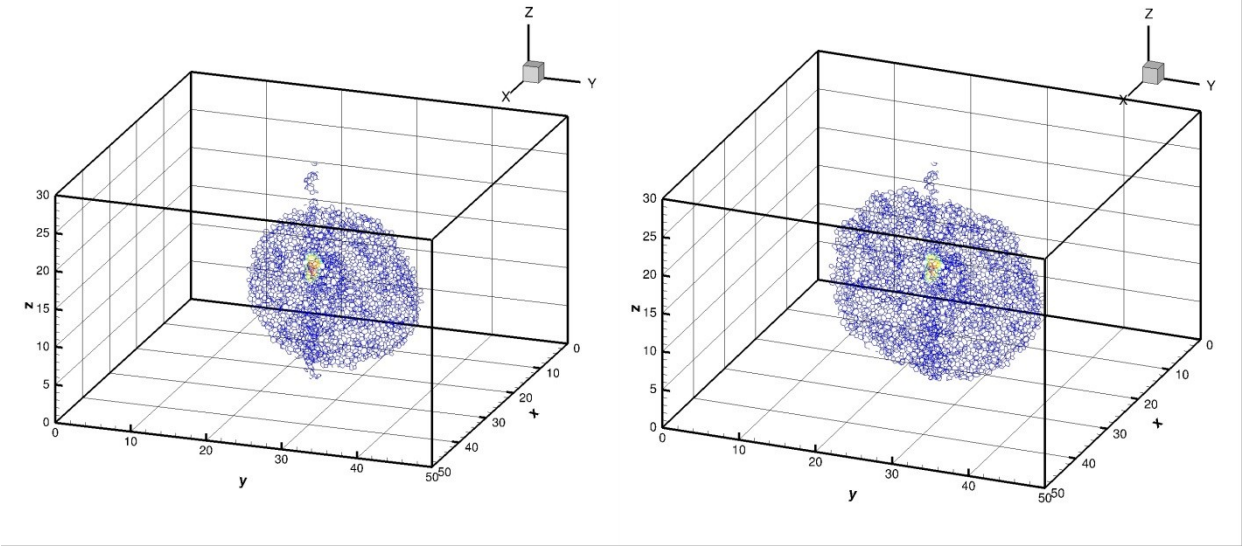

(c) t = 145 s (d) t = 345 s

Figure 5: Induced fracture geometry at different times. The color scales with the hydraulic diffusivity (warm and cool colors = high and low hydraulic diffusivity, respectively). Notice that the initial large hydraulic diffusivity within the injection zone, and the trend of reducing hydraulic diffusivity (which is equivalent to crack aperture) from near wellbore to the crack front.

Table 3. Generated fracture radius versus injection time and volume.

Injection Time (*s*)	Injection Volume (*liters*)	Crack Radius (*m*)
35 (Figure 5b)	1.17	1.21
145 (Figure 5c)	4.83	3.35
345 (Figure 5d)	11.5	4.26

The simulated fracturing pattern is further elucidated by examination of the stress field in the crack plane as depicted in Figure 6. The stress component S_{xx} shown here is actually the stress normal to the average crack plane (*YZ* plane). Note that we use a positive value for tension and negative value for compression (in contrary to the common geomechanics convention). There is a nearly circular ring with concentrated tensile stress, which actually represents the crack front, with a compressive stress zone within due to fluid pressing against the opened crack surfaces. It is these concentrated tensile stresses near the crack front that drive fracture propagation. It is obvious that the stress concentrations along the crack front are not uniform, due to the local variations of mechanical properties. Therefore the growth of the crack front is very much similar to the process of a moving contact line with random "pinning" and "de-pinning" (Måløy et al., 2006), which is a critical feature in order to generate episodic "bursts" of microseismic events.

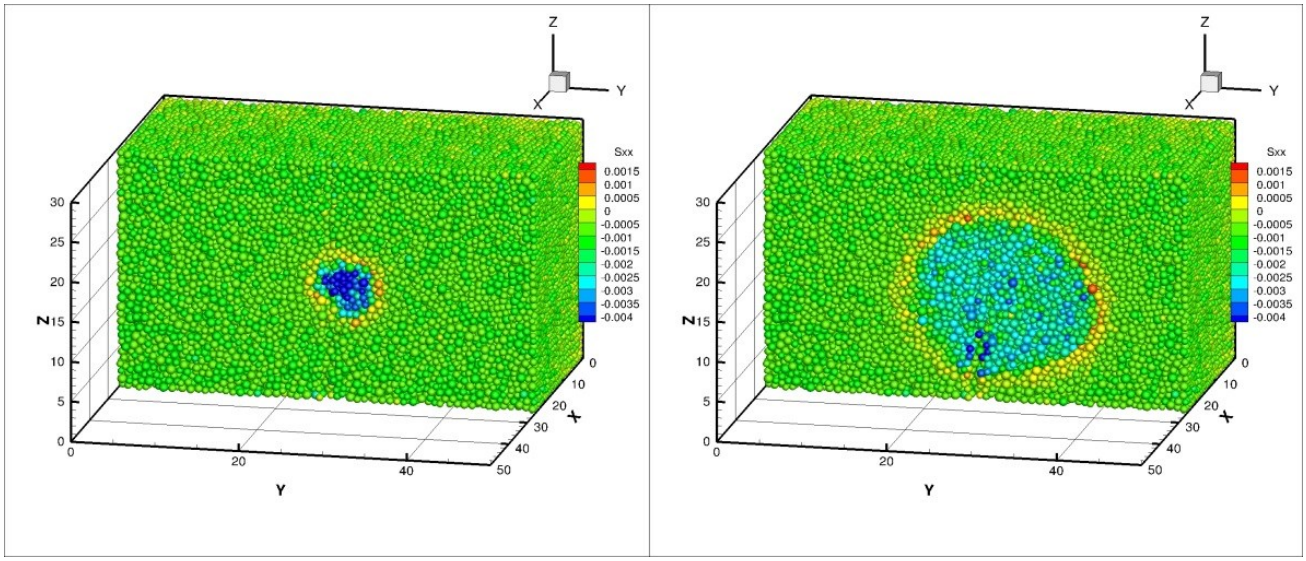

Figure 6: Dimensionless stress S_{xx} normal to the average crack plane during early (left) and (late) crack propagation stages.

Figure 7 shows the wellbore pressure evolution with injection time. From the simulation results, we observe that the fracture will start to propagate when the pressure reaches the peak defined by the breakdown pressure, and then it will propagate with a stable, reduced pressure called the propagation pressure. The estimated breakdown pressure is 66.78 *MPa*, and the estimated propagation pressure is 29.91 *MPa*. According to the literature (Yew, 1997), the breakdown pressure from analytical solution is:

$$P_b = 3\sigma_{Hmin} - \sigma_{Hmax} + T - P_0 = 3\square 25.07 - 30.35 + 29.3 = 74.16\ MPa \tag{9}$$

(with assumption of zero pore pressure) which is very close to the predicted breakdown pressure by the numerical simulations with the given initial *in-situ* stress conditions. However, due to a relatively large rock tensile strength value used in these pre-test simulations (carried out when the tensile strength was not known at the kISMET site), this predicted breakdown pressure provides an upper bound for wellbore breakdown pressure. In the simulated wellbore pressure vs. time curve, there is a rapid pressure decrease at ~35 seconds after the propagation starts, corresponding to the initial crack opening (a sudden increase in fracture volume to allow compressed fluid to rapidly expand). As the crack propagates farther, the fluid pressure needed to maintain crack growth decreases. According to fracture mechanics, a critical stress intensity value at the crack front (as a result of stress concentration at the crack front) needs to be reached and maintained in order to keep the fracture propagating. Because the stress intensity factor at the crack front is proportional to the square root of crack length, smaller fluid pressure acting against fracture walls are then needed to maintain a critical stress intensity value as the crack length increases.

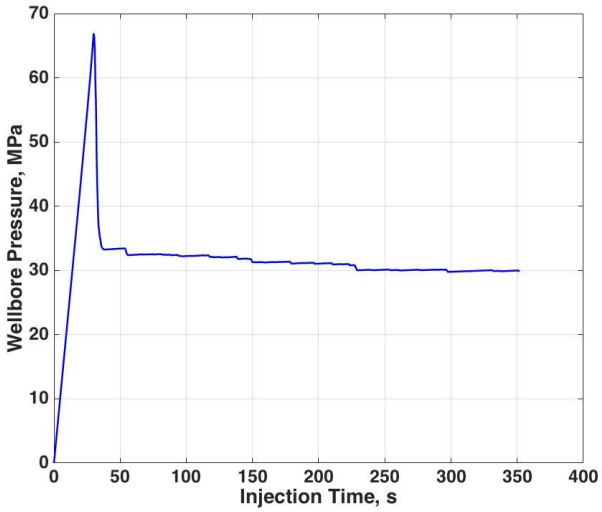

Figure 7: Wellbore pressure versus injection time.

5. ENERGY RELEASE

When the initial *in-situ* stress is applied in the model, strain energy is stored in elastic beams that connect DEM particles. As a crack initiates and starts to propagate, the beams will break due to the fluid injection and increase of pore pressure to model fracture initiation and growth. When this happens, the strain energy stored in the elastic beams will be released and partially converted into heat, partially absorbed by the neighboring DEM particles (via pressure-volume work), and partially radiated as elastic waves (i.e., as seismic waves) (Hazzard and Young, 2002).

One important concern that was raised by the physics experimental groups at SURF was how large the microseismicity would be from the hydraulic fracturing at kISMET. Therefore, one of the goals of the pre-test simulations was to provide an initial estimate of the magnitude of induced seismic events related to hydraulic fracturing at kISMET. The DEM model calculates the elastic strain energy released from the broken beams during simulated fracturing events. Assuming each beam breakage is a single seismic event, and further assuming all elastic strain energy stored in the beams prior to breaking is used in generating earthquakes, the DEM model then provides a very conservative estimate of the potential seismic magnitude.

Figure 8 gives a spatial-temporal map of the simulated seismic events and associated energies released. The events are colored according to time and sphere sizes are proportional to the event magnitudes. One general trend observed is that these simulated events are consistent with the crack propagation process, with earlier events closer to the wellbore, and later events farther away from the wellbore. Arguably, some earlier events with large energy releases are associated with initial crack opening and close to the wellbore. However, some large events far away from the wellbore are also observed during the late time. In general, the majority of the events are relatively small.

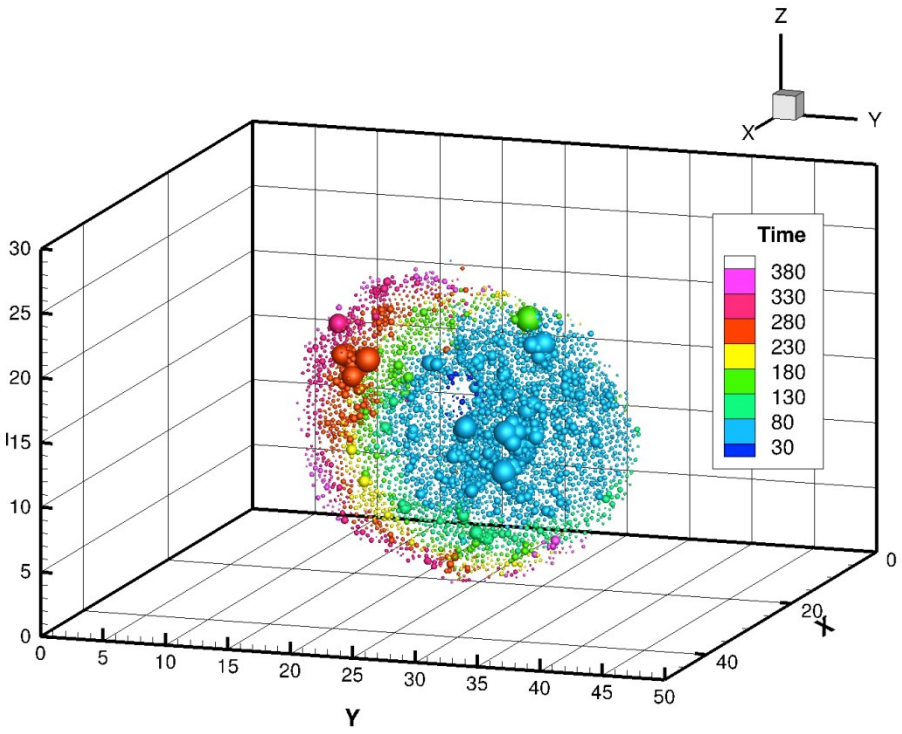

Figure 8: Seismic events generated by the coupled network flow-DEM model. The color of each sphere represents time and the size of sphere is proportional to event magnitude.

While the exact locations of individual events in the DEM model are meaningless because of the random perturbations added to the beam mechanical properties and the disordered DEM lattice that is used, the statistical temporal analysis of the released energies of individual events and cumulative released energy associated with fracture are more meaningful. Figure 9 shows the event energy release vs. injection time. We grouped the individual events during each time step into a single equivalent event. The largest energy release happened at the initial fracture opening stage, which has the most beam breakage events. After the initial opening, the fracture propagates smoothly (on average) under constant rate injection, with a few relatively large events (spikes shown in Figure 9**)**. The total energy released during the 345 *seconds* of injection is 0.37 *MJ*, and the average released energy of each event is 96.9 *J* (too small to be any concern of induced seismic hazard). The episodic bursts of events during the injection are actually a unique feature arising from incorporating local heterogeneity into the model.

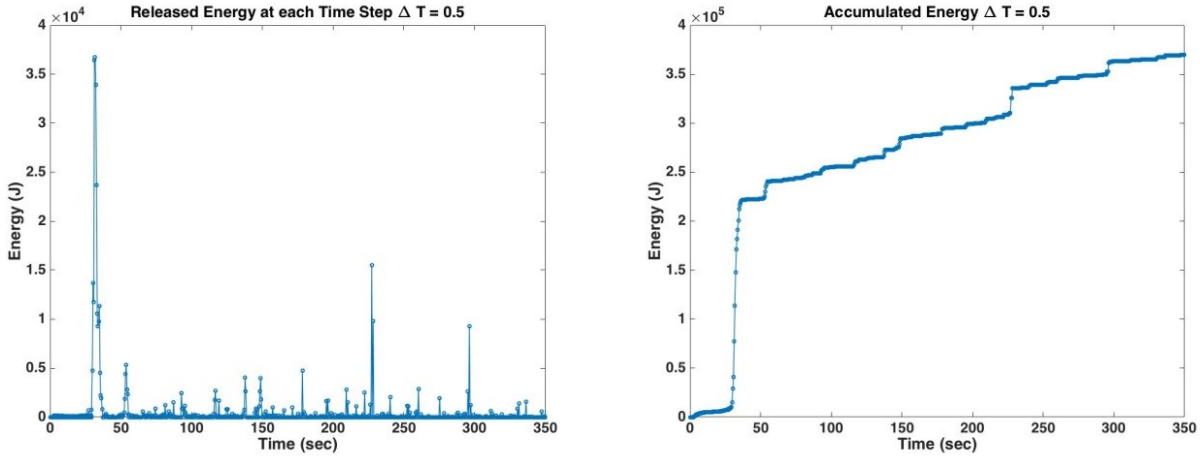

Figure 9: (Left) released energy vs. injection time and (right) cumulative released energy vs. time.

6. CONCLUSIONS

The coupled 3D network flow and quasi-static DEM model was successfully applied for pre-fracturing test simulations at the kISMET site to provide initial estimates of the breakdown pressure, propagation pressure, fracture geometry, which is very close to the value obtained from the post-test analytical calculations. Without an *in situ* stress gradient included into the model, the simulated hydraulic

fracture is similar to the penny shape crack expected for tensile hydraulic fracturing in an infinite homogeneous material. Due to the presence of local-scale mechanical heterogeneity incorporated into the DEM model, it is quite interesting to observe the random 'pining' and 'de-pining' of the propagating fracture front in the simulations. In addition, the pre-test simulation provides an initial estimate of the magnitude of induced seismic events related to hydraulic fracturing at kISMET. The majority of the events are very low-magnitude events, too small to be any concern in terms of induced seismic hazard).

In the follow-on modeling studies, we plan to recalibrate the model with actual core sample tests, and integrate the numerical simulation with better *in situ* stress data measured in the field in order to better understand the effect of rock fabric, stress anisotropy and pre-existing natural fractures on fracture propagation.

ACKNOWLEDGMENTS

Thanks are due to Alexandra Prisjatschew and Eric Hass (DOE Geothermal Technologies Office) for project management and encouragement. This work is supported by the SubTER Crosscut Initiative of the U.S. Department of Energy, and by Lawrence Berkeley National Laboratory under US Department of Energy Contract No. DE-AC02-05CH11231.

REFERENCES

Cundall, P.A., and Strack, O.D.: A discrete numerical model for granular assemblies, *Géotechnique*, **29**, (1979), 47–65.

Dahi-Taleghani, A., and Olson, J.: Numerical Modeling of Multistranded-Hydraulic-Fracture Propagation: Accounting for the Interaction Between Induced and Natural Fractures, *SPE Journal*, **16**, (2011), 575–581.

Economides, M.J., and Nolte, K.G.: Reservoir Stimulation, 3rd Edition, Wiley, (2000).

Fu, P., Johnson, S.M., and Carrigan, C.R.: An explicitly coupled hydro-geomechanical model for simulating hydraulic fracturing in arbitrary discrete fracture networks, *International Journal for Numerical and Analytical Methods in Geomechanics*, **37**, (2013), 2278–2300.

Hazzard, J.F., and Young, R.P.: Moment tensors and micromechanical models, *Tectonophysics*, **356**, (2002), 181–197.

Huang, H., and Mattson, E.,: Physics-based Modeling of Hydraulic Fracture Propagation And Permeability Evolution of Fracture Network In Shale Gas Formation, *Proceedings*, 48th US Rock Mechanics/Geomechanics Symposium, Minneapolis, MN, USA (2014).

Huang J, Yang C, Xue X, Datta-Gupta A. Simulation of Coupled Fracture Propagation and Well Performance under Different Refracturing Designs in Shale Reservoirs. In: SPE Low Permeability Symposium, Denver, Colorado, USA, 5-6 May, (2016).

Jing, L.: A review of techniques, advances and outstanding issues in numerical modelling for rock mechanics and rock engineering, *International Journal of Rock Mechanics and Mining Sciences*, **40**, (2003), 283–353.

Måløy, K. J., Santucci, S., Schmittbuhl, J., and Toussaint, R.,: Local waiting time fluctuations along a randomly pinned crack front, *Physics Review Letter*, **96**, (2006), 1–4.

Oldenburg, C.M., P.F. Dobson, and 30 others, Intermediate-Scale Hydraulic Fracturing in a Deep Mine, kISMET Project Summary 2016, Lawrence Berkeley National Laboratory Report, LBNL-1006444, (2016).

Potyondy, D. O., and Cundall, P. A.,: A bonded-particle model for rock, *International Journal of Rock Mechanics and Mining Sciences*, **41**, (2004), 1329–1364.

Vigilante, P.,: Critical Review of Laboratory Rock Properties and State of Stress in the Sanford Underground Research Laboratory (SURF), (2016).

Wu, K., and Olson, J.E.,: Investigation of the Impact of Fracture Spacing and Fluid Properties for Interfering Simultaneously or Sequentially Generated Hydraulic Fractures, *Conference*, SPE Hydraulic Fracturing Technology Conference, Woodlands, Texas, USA (2013).

Xu, W., Thiercelin, M., Ganguly, U., Weng, X., Gu, H., Onda, H., Sun, J., and J.L. Calvez,: Wiremesh : A Novel Shale Fracturing Simulator Models, *Proceedings*, International Oil and Gas Conference and Exhibition in China, 8-10 June, Beijing, China (2010).

Yew. C.H.,: Mechanics of Hydraulic Fracturing, Gulf Publishing Company, Houston, Texas (1997).

Zhou, J., Huang, H., and Deo, M.: A New Physics-Based Modeling of Multiple Non-Planar Hydraulic Fractures Propagation, *Conference*, Unconventional Resources Technology Conference, San Antonio, Texas, USA (2015).